Available online at http://www.ijprt.org.tw/

Chinese Society of Pavement Engineering

International Journal of Pavement Research and Technology 11 (2018) 819-828

http://www.ijprt.org.tw/

Sealing of paving stone joints

Mauro Coni *, Silvia Portas, Francesca Maltinti, Francesco Pinna

DICAAR, Department of Civil Engineering, Environment and Architecture, Faculty of Engineering, University of Cagliari, Via Marengo 2, 09123 Cagliari, Italy

Received 31 October 2017; received in revised form 26 June 2018; accepted 1 July 2018

Abstract

This paper reports an experimental analysis of the joint-sealing material of stone pavement subjected to a heavy load in an urban context. Joint sealing is needed to avoid water intrusion and to prevent pumping phenomena. According to a literature review, the sealing process improves the structural behavior, interlocking, and roughness. Paving stone irregularity affects safety in particular for bikes and motorbikes. The traditional use of cement slurries has short-term benefits due to their rigid and brittle behavior, while the use of asphalt sealants is often incompatible with the desired esthetic quality. A novel sealing technique was tested during the resurfacing of a historic stone pavement in the waterfront of the city of Cagliari (Italy). Laboratory four-point bending tests and finite element (FE) simulations were conducted on prismatic specimens obtained by connecting sealing material and granite samples. FastFWD on the newly sealed stone pavement validates the laboratory results and numerical simulations. The results demonstrate the benefits of the novel sealing technique: high bonding capacity, better distribution of stress, greater interlocking and minor relative displacements between stone elements. The load transfer efficiency (LTE) between blocks is increased from a mean of 84% for sand-cemented joints to 95.5% for the new resin joints, while the stress is 28% less.

Keywords: Paving stone; Joint; Sealing; Historical pavement; FEM simulation; Load transfer efficiency

1. Introduction

Different types of stone pavements are widespread in historic areas, and there are increasing amounts of new construction and requalification (Fig. 1). Paving blocks can be made of a variety of materials to satisfy functional and esthetic quality standards [1–3].

However, there is no theoretical method to analyze assembled discontinuous structures, such as block pavements [4]. Therefore, the finite element method (FEM) has potential to investigate the mechanical behavior. The structural and functional performance depends on the type of joint and the dynamic load amplification, which is triggered by roughness. Joint shape and thickness, sealing material and block patterns also affect overall pavement efficiency [5–8].

The joints of the historical stone pavement are typically not sealed; however, sealing materials have been applied in the past 50 years to increase the bearing capacity due to increased traffic. Joints are generally sealed with cementitious or bituminous mortars to prevent water intrusion and pumping and to improve interlocking [3,9,10]. Unsealed joints have significantly higher capacity than damaged sealants, and sealants are less effective when there are extreme joint openings [11]. The pavement roughness has a significant adverse impact on the bikers and motorbikes' stability. Also, the pedestrian accident due to unevenness in stone surfaces is well known and reported [12–15].

* Corresponding author.
E-mail addresses: mconi@unica.it (M. Coni), sportas@unica.it (S. Portas), maltinti@unica.it (F. Maltinti), fpinna@unica.it (F. Pinna).
Peer review under responsibility of Chinese Society of Pavement Engineering.

https://doi.org/10.1016/j.ijprt.2018.07.002

Fig. 1. Different types of stone pavements: sett, cobblestone, flagstones.

The use of sand-cement mortar creates a rigid and fragile joint that quickly cracks and detaches [16–17]. Bituminous materials have a better mechanical performance than cement mortar, but they are incompatible with the historical context and esthetic quality. Neither solution significantly affects the overall mechanical performance because they do not ensure significant load transfer efficiency between adjacent stone elements. Particularly relevant are the dynamic effects generated by moving loads on the irregularities of the stone elements and joints.

The stone pavement in the historic waterfront of the city of Cagliari is frequently subjected to maintenance to restore disconnections between stones due to joint weakness (Fig. 2). The pavement is composed of blocks of granite squared in irregular prisms with maximum dimensions of 40 × 80 × 19 cm. The elements are set in a herringbone pattern with regular plots and characterize the valuable areas of many historic towns and villages in Italy. A granular foundation layer and cement treated base layer support the blocks and fill the underneath irregularity. Typically, the cement mortar sealed the spaces between the blocks. The overall mechanical behavior of the pavement is complex: highly rigid locally but flexible on a macroscopic scale.

The stone pavement technique, developed by the Romans, has improved since 1700. The high hardness of the stone was essential to resist the passage of metal wheels and to avoid the formation of trenches, while the inertia of the heavy elements guaranteed stability and planarity over time.

These pavements offer many benefits [1]: high esthetic value and compatibility with the historical context; better resistance to weather; limited phenomena of fatigue, rutting, potholes and cracks; and lower surface maintenance costs. However, there are also some disadvantages: higher costs and construction complexity; greater noise and vibration [18]; less skid resistance; and vehicle passenger discomfort. Joint failure is the main weakness of the block pavement. Water intrusion reduces bearing capacity, interlocking and load transfer between adjacent elements, resulting in more frequent block movement and rotation [19–22].

2. Case study

The flagstone pavement of the Cagliari waterfront (Fig. 2, top left) was built in 1870, and it is currently protected as a monument and landscaped site. The street is one of the primary connections between the western and eastern parts of the metropolitan area, with 1800 vehicles/h in peak hours, 25% of which is heavy vehicles, mainly urban buses. The traffic creates frequent disconnections requiring maintenance activity. A critical event occurred in 2014. The fast passage of a bus dragged some of the

Fig. 2. The flagstone pavement on the Cagliari waterfront and typical distress.

Fig. 3. The critical event in November 2014 and bearing capacity survey.

heavy elements out of place (Fig. 3), projected the bus upward and wounded several passengers. The technical survey points out the low efficiency of the joints relative to the dynamic loads induced by the transit loads and water intrusion. In this case, several effects contribute to instability: unbounded subgrade materials can change the bearing capacity, the dynamic load activates a water pore pressure transmitting the stress, and the pumping effect can remove sand support. The survey indicates rainwater intrusion, due to crack of the joint, as the main reason for pumping and disintegration of the sand-cemented underlying material. This layer loses the bound capacity and finally appears as unbounded granular materials.

All joints, filled with sand-cement, mortar featured widespread disconnections, fragile breakage, and erosion. Several flagstones oscillated when they were loaded asymmetrically, even with limited weights. An exploration trench and load plate tests were used to evaluate the thicknesses (Fig. 4), the residual bearing capacity of the subgrade and subbase layers, the support material quality and, finally, to define the intervention plan.

Static load plate tests were performed on base layer after flagstone removal. The tests are widely used in Italy to determine the deformation modulus (Md), applying vertical stress, throw a circular plate of 30 cm diameter (d), and measuring the vertical displacement (δ). Md denotes the slope of the secant of $\sigma_v - \delta_v$ curve by the formula:

$$M_d = \frac{\Delta\sigma_v}{\Delta\delta_v} d$$

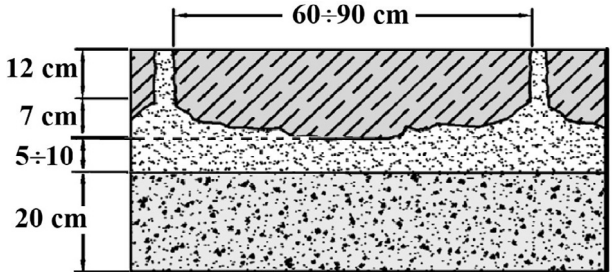

Fig. 4. Stone pavement geometry.

where Md is the deformation modulus in MPa, d is circular plate diameter in mm, $\Delta\sigma$ is the change in stresses from 0.25 to 0.35 MPa, $\Delta\delta$ is the change in a measured deflection in mm.

The dirty surface of the stone elements can affect adhesion of joint-sealing material. Thus, the flagstones are cleaned first removing mechanically cement-sand attached material and, just before the application, with high-pressure jet water (Fig. 5). A new technique to seal joints using epoxy resins was tested in the right lane (4.50 m width, 500 m length).

A proper bearing capacity value, with average Md of 102.4 MPa, was found during the survey. Therefore, attention was focused on the underlying material and sealing joints. The implemented technique involved the following steps: (1) catalog and displace the flagstones; (2) remove the cement-sand deteriorated layer; (3) add new sand-cemented material and a metal mesh; (4) reposition the pre-existing flagstones, and (5) seal with the epoxy material (Fig. 5). Historical and Monumental Protection Authority supervised all phases of the pavement restoration.

Due to the irregularity of the stone elements, the joints are not perfectly prismatic but taper toward the surface, with a variable thickness from 10 mm to 40 mm. The bicomponent epoxy resin has a granular siliceous matrix with adequate mechanical and fatigue properties (Fig. 6).

3. Research methodology

The study aimed to evaluate the structural capacity of the joints and to estimate the improvements of the stress and strain fields. Eight prismatic specimens at the joint were subjected to repeated cycles of the four-point bending test (4PBT). The new pavement was tested with 42 deflectometric drops performed with the FastFWD at three stress levels to evaluate the ability of a deflection basin with a specific geophonic configuration to return the load transfer efficiency (LTE) between adjacent elements. Finally, a series of FE simulations of the 4PBTs and the 2D pavement section subjected to the FWD dynamic load were conducted (Fig. 7).

Fig. 5. Removal of the cement-sand deteriorated layer, cleaning, and joint sealing.

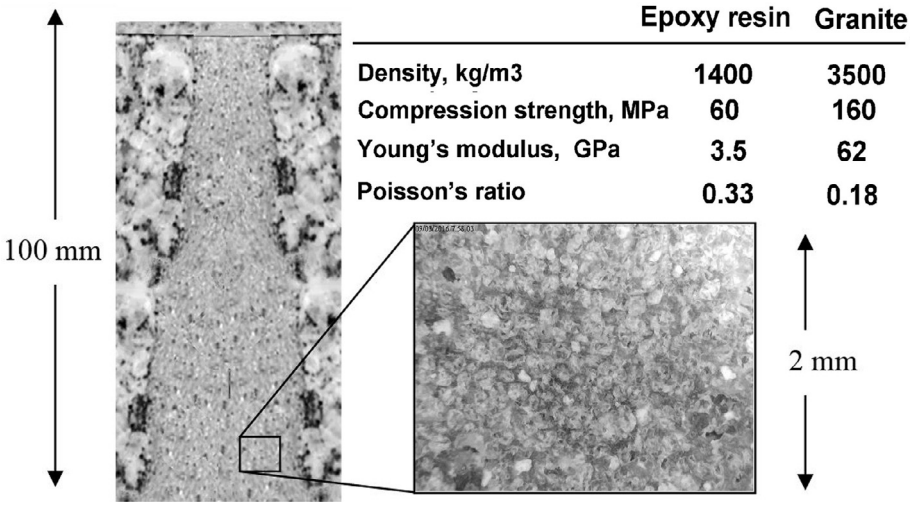

Fig. 6. Details of the joint shape and granular siliceous matrix.

Fig. 7. (a) 4 point bending tests (4PBT); (b) FastFWD tests; (c) FEM simulations.

The specific research objectives have been: (a) to determine the LTE between flagstones; (b) to evaluate the influence of the thickness of the joint; (c) to analyze whether the underlying material deficiency affects the LTE; (d) to estimate whether the block irregularities and joint shape affect the LTE, and (e) to assess the overall behavior of the new pavement relative to the old pavement.

4. Four-point bending test in the laboratory

The origin of joint degradation is fatigue phenomena induced by the repetition of loads. Fatigue investigation was conducted via 4PBTs using prismatic specimens (137 × 42 × 42 mm) sawn from two adjacent pavement blocks glued together with epoxy resin. The 4PBT frame was designed to reproduce the beam pattern: two lateral supports and two forces applied symmetrically at L/3 beam length (39 mm). A Nottingham Asphalt Tester (NAT) was used for the fatigue analysis, and a load transfer system and Linear Variable Differential Transformer (LVDT) sensors were used to measure the stress and horizontal and vertical deformation. The NAT is designed for cylindrical specimens of diametrically loaded bituminous conglomerate; thus, to connect the frame to the testing machine, special pieces were manufactured to fit the actuator and reaction plate. Furthermore, a 4PBT rig permits to measure the vertical movement at the neutral axis of the specimen (Fig. 8). The 4PBTs, set in strain control, allow measuring the deflection of the central part of the specimen at a specific strain level, and calculating σ_t and ε_t using the following equations:

$$\sigma_t = \frac{P \cdot l}{b \cdot h^2} \qquad \varepsilon_t = \frac{108 \cdot \delta \cdot h}{23 \cdot l^2 + 36 \cdot h^2 (l + v)}$$

where σ_t = tensile stress (Pa); P = load amplitude applied to the specimen, $(N) = P/2$ on each loading point; l = beam span (m); b = beam width (m); h = beam height (m); ε_t = applied tensile strain (m/m); δ = beam deflection at the neutral axis (m); and v = Poisson's ratio. Based on these relationships, the modulus E for each cycle of the test was:

$$E = \frac{\sigma_0}{\varepsilon_0}$$

The equipment allows temperature's and frequency's adjustment and the actuator set the repetition rate of the load.

Fatigue tests were performed on five prismatic specimens with a nominal tensile stress of 1.67 MPa applied to the specimen. Granite flagstone samples were cut, sealed with resin, squared and rectified in the laboratory. The same process was not possible on joints sealed with sand-cement mortar because the cutting and preparation operations destroyed the samples, demonstrating the low adhesive capacity and fragility of joints made with sand-cement mortar.

The tests performed on the resin joint specimens showed 3 phases (Fig. 9). After the first linear phase (<5000 cycles), the deflections progressed at a decreasing rate. Afterward, the curves evolved linearly up to 100,000 cycles.

An exponential trend was observed before collapse (approximately 112,000 cycles for all specimens). The specimens have a joint thickness ranging from 27 mm to 42 mm. The imposed stress produced a 0.28 mm maximum deflection, which was stable for the first 100 cycles for all specimens. Narrow joints exhibited smaller permanent deformation ε_{up}, which grew as a function of joint thickness and the number of cycles, reaching similar values in all cases at collapse. The number of cycles at collapse was the same for different joint thicknesses, while different behavior appeared starting in the first phase.

The broken surface occurred at the granite/mortar interface in all specimens, sometimes with a detachment of quartzite particles from the granite contact surface since quartzite is the weakest element of the two materials.

5. FWD tests in situ

The deflectometric survey was conducted by use of FastFWD (Dynatest FastFWD Model 8012). The test is conventionally performed on flexible, semi-rigid and rigid pavements and can be extended, with some caution, to segmented pavements [23,24]. FastFWD is designed to be faster than the FWD, and it can impart a load pulse to the pavement surface to simulate the load produced by a moving vehicle. The load cell measured the load pulse with a resolution of 0.1 kPa, and 15 deflection sensors record the pavement response with a resolution of 0.1 μm.

The measurements showed an unconventional deflection basin with a narrow bending between 200 and 450 mm from the plate center. This measurement depends on the plate position relative to the joints. Deflections close to

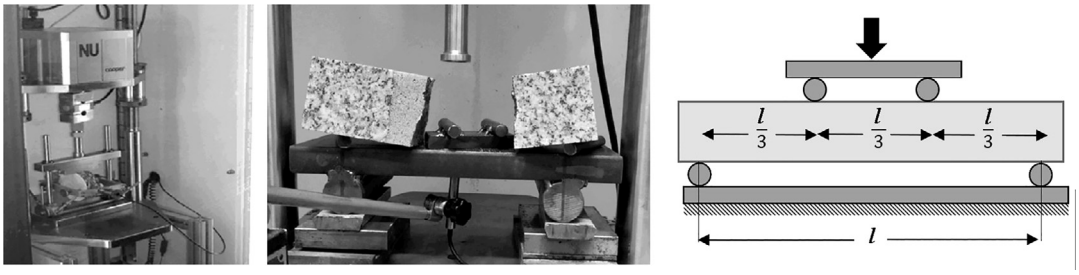

Fig. 8. Adapted NAT equipment, fatigue breakage and 4PBT scheme.

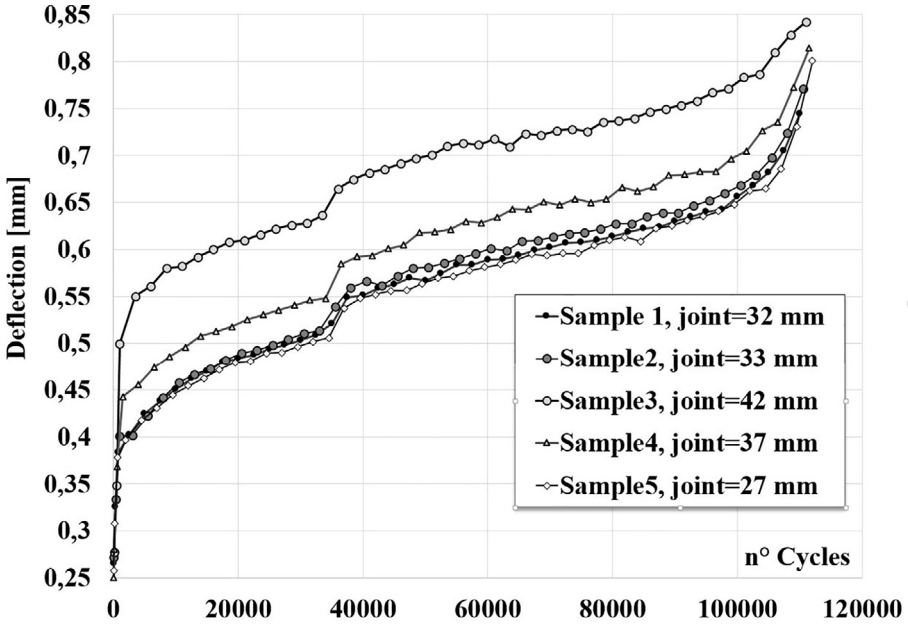

Fig. 9. Results of the four-point bending fatigue tests.

the plate (D-150, D-300, D-200, D-300 and sometimes D-450) tend to replicate D0 owing to the high local stiffness of the basin relative to global behavior.

The post-processing software (Dynatest ELMOD 6) was used to back-calculate the pavement layer elastic modulus based on the impact load and surface deflection basin using Odemark-Boussinesq theory. The iterative method "Deflection Basin Fit" provides the best combination of stiffness and thickness and minimizes the deflection deviation between the model and the detected data. This back-calculation method provides good correlations between the measured and predicted strains and stresses in the pavement structure and thus gives an accurate pavement response [25,26].

Direct tests estimated the elastic modulus of the subgrade the elastic modulus of the subgrade on undisturbed samples taken at different depths of up to 8 m. The mean value was 22 MPa. Fig. 10 shows the geophone configurations and the deflection basins. Forty-two FastFWD tests (one every 40 m) were performed.

The joint load transfer capacity was evaluated according to the ratio between the displacement of two nearby geophones near the loading plate. The LTE was used to express the ability of a joint to transmit the load from the slab to the adjacent unloaded slab [27–29]. Several formulae are used to evaluate LTE, but LTEδ (deflection load transfer efficiency) remains the most common [30,29,31].

$$LTE_{\delta} = \frac{\delta_{unloaded}}{\delta_{loaded}} 100$$

The load plate configuration is variable concerning the plan pattern of the joints, as shown in Fig. 11.

However, considering the orientation, element size (0.40 × 0.80 m) and the load plate diameter (0.30 m), at least one of D + 200 and D − 150 transducers occurs in the flagstone adjacent to the flagstone loaded with the FWD plate.

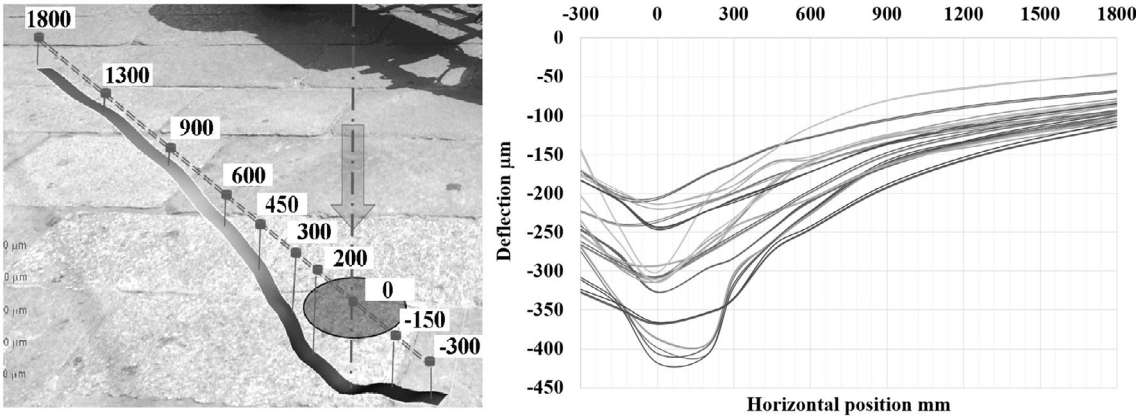

Fig. 10. FWD transducer configuration and deflection basin envelope for the 42 drops.

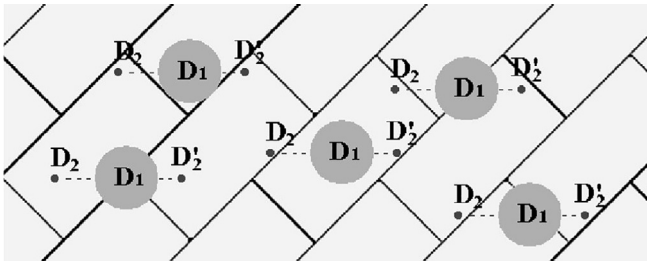

Fig. 11. Different load plate positions on the joint configurations.

Therefore, the lower value between D + 200/D0 and D − 150/D0 indicates the joint efficiency. The average of this value for 42 drops was 84.7%.

6. Finite element analysis

The stress and deformation fields were investigated with two different FE models. First, the laboratory 4PBTs were simulated with a 3D model [31]. A second simulation was conducted to reproduce the behavior of a 2D section of the stone pavement (2.40 m width and 2.50 m depth). The two models, developed in an elastic field, were calibrated using the results obtained from the in situ and laboratory tests (Fig. 12).

The prismatic specimen used for the 4PBT model had dimensions of 137 mm × 42 mm × 42 mm and was formed with three volumes, 2 simulating the two stone portions joined with a volume of the epoxy resin. The load points and constraints reproduced the geometry of the laboratory tests. Since the break surface observed in laboratory occurred at the interface between the epoxy resin and granite, the FE model incorporated a thin section to better approximate the contact surface. The 3D model used a SOLID 45 element consisting of 8 nodes, each with 6 degrees of freedom. The model was calibrated step by step by introducing the typical nominal values of the materials shown in Fig. 6 in the first phase. The objective was to reproduce the maximum deflection obtained in the laboratory at the 100th cycle in 4PBTs fatigue tests (284 μm). The calibrated model was used for parametric analyses by modifying the joint geometry. A PLANE42 element, consisting of 4 nodes, each with 3 degrees of freedom, was used in the 2D pavement model. The model was constrained with zero vertical displacements on the bedrock and zero horizontal movements in the lateral boundaries. The impulsive vertical load (100 kN, 30 ms) was applied to the central nodes to reproduce the FWD load configuration. The objective of the calibration was to minimize the variance between the simulated and FWD-measured basin deformation [32–35].

6.1. FE results

The 4PBT 3D FE simulations included different joint sizes (7–37 mm) and shapes (wide or narrow on the top, very wide or very narrow on the top, vertical sides). In the vertical and parallel joints, the simulated deflections grew linearly with thickness up to 26 mm and became exponential at higher values, as shown in Fig. 13. The figure also shows the trend of the horizontal stress, which exhibited small changes as the joint thickness increased.

The joint efficiency remained stable (1.2% for the joint with resin and 2.0% for sand-cement mortar) when varying the subgrade stiffness between 50 and 120 MPa, whereas varying the thickness resulted in high differences. Tight and regular joints had the best values, while large and irregular joints had approximately 11.5% lower efficiency. Resin-sealed pavement showed better overall behavior with a more homogeneous distribution of the stress state. The equivalent stress reached maxima of approximately 1.17 MPa and 1.62 MPa in joints with the epoxy resin sealing and sand-cement mortar, respectively (Fig. 14).

The LTE was also estimated through 2D FE pavement simulations. The loading plate was moved along the flagstone to obtain the LTE value for each position. When only one load cycle was applied, and the joint was sealed with resin, the average LTE was 95.1%, whereas the average was 88.5% for joints sealed with cement mortar. After 10,000 cycles (stress equivalent of approximately 85% of the tensile stress used in the laboratory for the prismatic specimens), the LTE for sand-cement mortar joints decreased significantly to 69.9%, while that of resin-sealed joints decreased to 93.5% (Fig. 15).

The difference (~10%) between the LTE estimate from the FWD measurements (84.7%) and the FE result (95.1%) can be explained by the lack of elastic behavior of the real materials and the imperfect coupling between

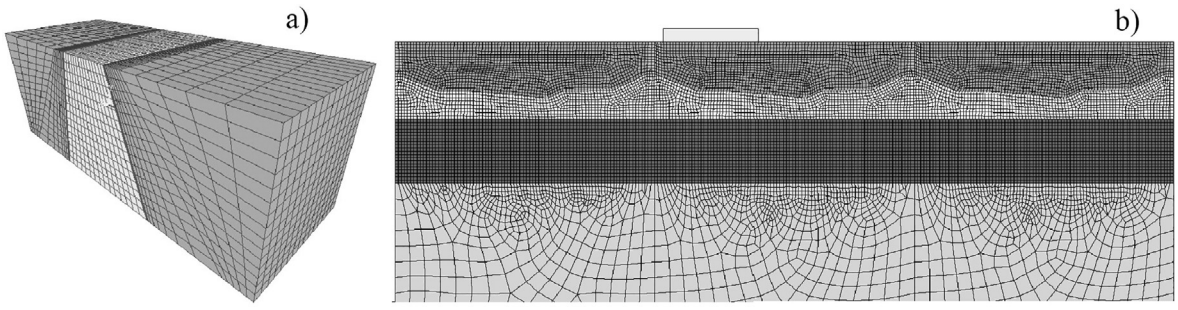

Fig. 12. (a) 3D prismatic specimen of the four-point bending test; (b) 2D section of the stone pavement under the load plate.

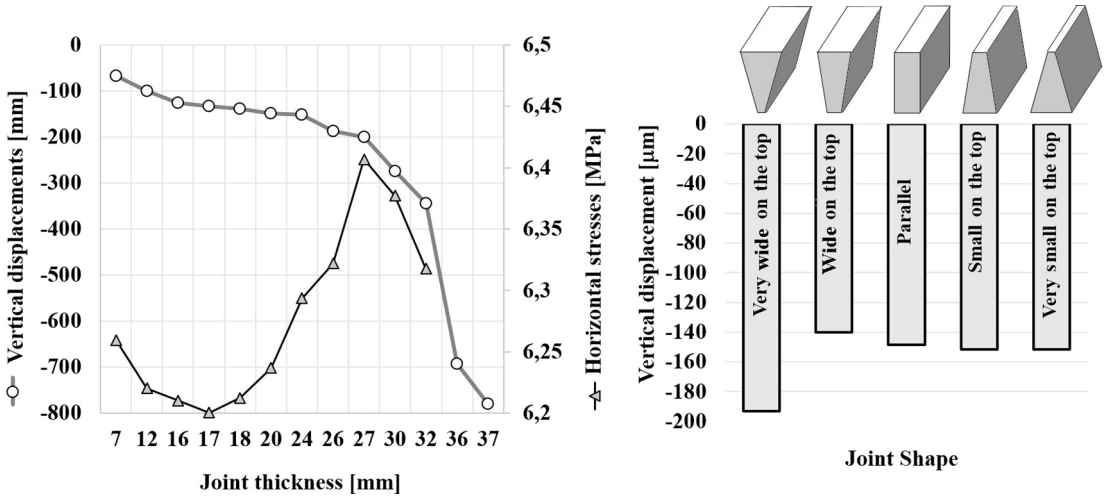

Fig. 13. Vertical deflection and horizontal stress vs. thickness and joint shape.

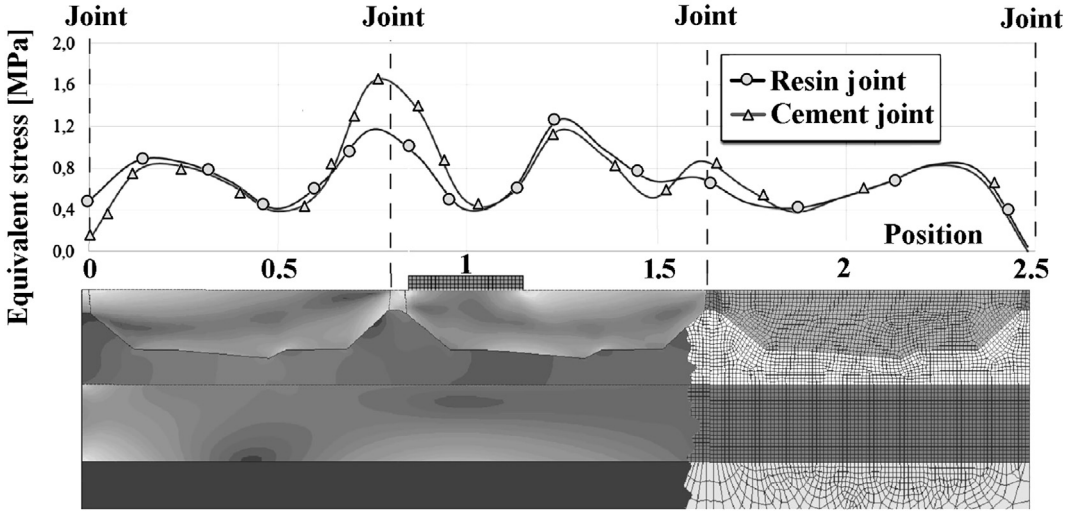

Fig. 14. Equivalent stress in the pavement with cement and resin joints.

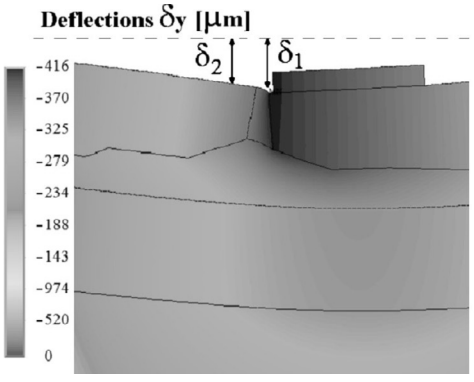

JOINT EFFICIENCY $J_{eff} = \frac{\delta_1}{\delta_2} \cdot 100$

	Resin joint	Cement joint
FWD measurament	84,7%	63,4% *
FEM simulation 1 cycle	95,1%	88,5%
FEM simulation 10.000 cycles	93,5%	69,9%

** estimated value*

Fig. 15. Joint efficiency, FWD measurements, and FE simulation.

the flagstones and the support layer. Likewise, for a pavement sealed with cement mortar, the expected value of 63.4% was less than 10% of the value obtained by the FE simulation. The LTE decreased from 97.5% to 89.5% when the resin joint size was increased from 8 mm to 48 mm. Smaller variation, ranging from 97.7% to 90.7%, resulted in a poor subgrade (Figs. 16 and 17). With sand-cement joint sealing, LTE ranged from 96.2% to 84.3% on a good

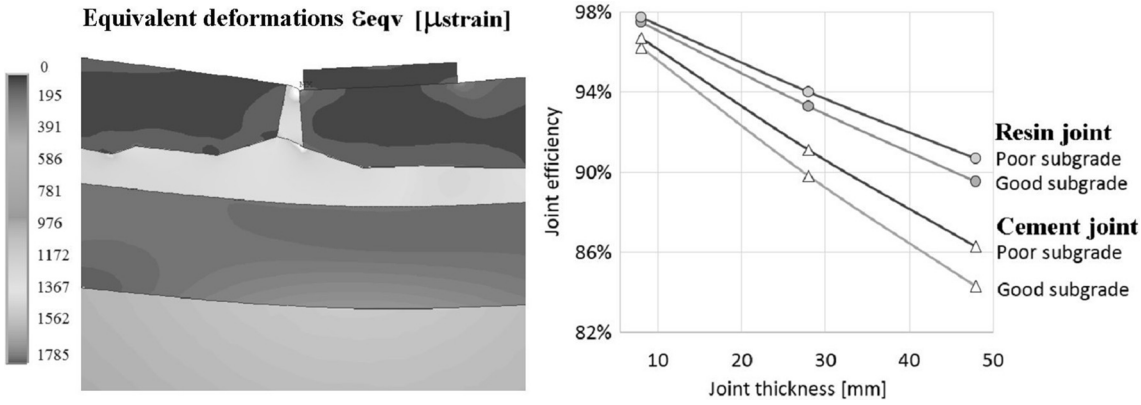

Fig. 16. Equivalent deformation distribution and LTE vs. joint thickness and subgrade stiffness.

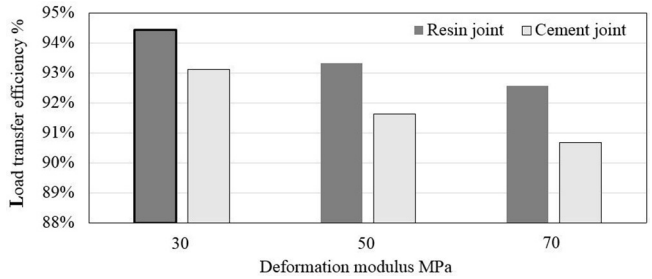

Fig. 17. Joint efficiency vs deformation modulus (joint thickness 28 mm).

subgrade and from 96.7% to 86.3% on a poor subgrade. The deformation modulus ranged from poor, with Md = 30 MPa, to good with Md = 70 MPa.

7. Conclusion

Stone pavement joints composed of sand-cement mortar have low adhesive capacity and fragility. A new technique to seal stone pavement was assessed on a full-scale test section of the historic pavement on the waterfront of the city of Cagliari. Laboratory 4PBTs and FE simulations were also conducted to evaluate the structural capacity of the epoxy resin joints. The results demonstrated that the novel sealing joints could improve stone pavement performance. The following conclusions are drawn from the results of the tests and FE simulations:

- In resin joints, the LTE decreases as the thickness increases. The 4PBT specimens with narrow joints exhibit smaller deflections;
- The number of cycles to fatigue failure remains constant as the thickness increases;
- The broken surface occurs at the interface between the granite stone and epoxy resin, sometimes with a detachment of granite quartzite particles;
- LTE is a complex parameter that depends mainly on the joint thickness. Large and irregular joints decrease LTE by approximately 12%;
- The subgrade bearing capacity has a relatively weak effect on joint efficiency;
- The equivalent stress shows low variability as the thickness increases;
- The LTE estimated by FWD is 84.7%. The FE modeling of the first load cycle gives values of 95.1% and 88.5%, respectively, for resin-sealed joints and cement mortar. After 10,000 load cycles, the values decrease to 93.5% and 69.9%. The difference between the FWD measurements and FE modeling can be explained by the elasticity of the materials and perfect layer coupling;
- The better behavior of the resin-sealed joints is due to the more homogeneous distribution of the stress state.

Finally, the paper analysis is limited to stress and fatigue induced by transit load, not taking into account thermal stress and thermal cycling. Further research could investigate these aspects, which can affect long-term performance.

Acknowledgments

Road Department of the Cagliari Municipality in Italy support the research. The authors would like to acknowledge Dr P. Piastra, Dr. E. Passa and Dr. R. Piras for their technical support during the in situ investigations.

References

[1] Advise Series, The Conservation of Historic Ground Surfaces, Dublin City Council, ISBN 978-1-4064-2837-7, 2015.
[2] Guidance Notes on Design and Construction of Pavements with Paving Units, Hong Kong Highways Department, Research & Development Division, October 2014.
[3] G. Blanco, Pavimentazioni in Pietra, Ed. Carocci, Roma 1994.
[4] T. Nishizawa, S. Matsuno, M. Komura, Analysis of interlocking block pavements by finite element method, in: Proceedings II International Conference on Concrete Block Paving, Delft (NL), 1984.
[5] Houben L.J.M., A.A.A. Molenaar G.H.A.M. Fuches, and H.O. Moll, Analysis, and design of concrete block pavements, in: Proceedings II International Conference on Concrete Block Paving, Delft (NL), 1984.
[6] M. Crispino, Analisi di caratteristiche funzionali e strutturali di pavimentazioni in Pietra a Maselli, X Convegno Nazionale S.I.I.V, Catania Ottobre, 2000.
[7] M. Coni, J. Knapton, R. Senes, F. Annunziata, FEM simulation and experimental analysis of block pavements in airfield apron, in:

Proceedings IX Conference S.I.I.V. (Italian Society of Transport Infrastructures), Cagliari (IT), 1999.
[8] E.I. Aghimien, D.O. Aghimien, I.A. Awodele, Assessment of the use of solid concrete and interlocking stones in the construction of walkways in a tertiary institution, civil and environmental research, www.iiste.org ISSN 2224-5790 (Paper) ISSN 2225-0514 (Online) 8(9), 2016.
[9] J. Chehovits, M. Manning, Materials and methods for sealing cracks in asphalt concrete pavements, Transportation Research Record, Issue Number: 990 Sealing bridge and pavement joints, ISSN: 0361-1981, 1984
[10] B. Odum-Ewuakye, N. Attoh-Okine, Sealing system selection for jointed concrete pavements, Constr. Build. Mater. 20 (8) (2006) 591–602.
[11] K. Neshvadian Bakhsh, D.G. Zollinger, Y. Jung, Evaluation of joint sealant effectiveness on moisture infiltration and erosion potential in concrete pavement, in: Proceedings Transportation Research Board 92nd Annual Meeting, 2013.
[12] NCHRP Project 20 68A, Scan 09 04 Leading Practices for Motorcyclist Safety, National Cooperative Highway Research Program, September 2011, http://onlinepubs.trb.org/onlinepubs/nchrp/docs/nchrp20-68a_09-04.pdf.
[13] F. Bella, A. Calvi, F. D'Amico, Impact of pavement defects on motorcycles' road safety, Procedia Soc. Behav. Sci. 53 (3) (2012) 942–951, https://doi.org/10.1016/j.sbspro.2012.09.943.
[14] J. Eubanks, P.F. Hill, D.A. Castee, Pedestrian accident reconstruction and litigation ISBN-13: 9780913875254, Lawyers and Judges Publishing January 30, 2004.
[15] M. Crispino, A. Tasora, E. Vaghi, Analisi della pericolosità della marcia dei veicoli a due ruote su pavimentazioni lapidee irregolari. http://www.projectchrono.org/tasora/pubblicazioni/aosta2003_bike.pdf.
[16] T.D. Biel, H. Lee, Performance study of Portland cement concrete pavement joint sealants, J. Transp. Eng. 123 (5) (1997).
[17] M. Crispino, L. Venturini, Analisi sperimentale su resine poliuretaniche monocomponenti per la sigillatura delle pavimentazioni a masselli in pietra, XI Convegno Nazionale S.I.I.V, Verona, 2001.
[18] L. Domenichini, R. Ferro, F. La Torre, Vibrations produced by road traffic influence of the road surface characteristics, International Symposium on the Environmental Impacts of Road Pavement Unevenness (SIAIS), Porto, 1999.
[19] M.G. Lay, Handbook of road technology, Fourth Ed., CRC Press, 2009.
[20] S.F. Shober, Portland cement concrete pavement performance as influenced by sealed and unsealed contraction joints, Transp. Res. Rec. (1986), n1083, ISSN: 0361-1981.
[21] S.D. Tayabji, B.E. Colley, Improved rigid pavement joints, Transp. Res. Rec. (1983), 930 ISSN0361-1981
[22] B.J. Dempsey, Q.L. Robnett, Influence of precipitation, joints, and sealing on pavement drainage, Transp. Res. Rec. (1979), n705, ISSN: 0361-1981.
[23] R.J. Armitage, Concrete block pavement evaluation with the falling weight deflectometer, in: Proceedings Third Int. Conf. on Concrete Block Paving, Rome (IT), 1988.
[24] L. Khazanovich, A. Gotlif, Evaluation of Joint and Crack Load Transfer Final Report October 2003, FHWA-RD-02-088, source at https://www.fhwa.dot.gov/publications/research/infrastructure/pavements/ltpp/reports/02088/02088.pdf
[25] Guidance notes on backcalculation of layer moduli and estimation of residual life using falling weight deflectometer test data, Hong Kong Highways Department, Research & Development Division, RD/GN/027A, June 2009.
[26] H.L. Von Quintas, A.J. Bush, G.Y. Baladi, Nondestructive testing of pavement and back-calculation of moduli, Ed. ASTM PCN 04-01198008 1198, Dec. 1994.
[27] Z. Yan-cong, G. Ling-ling, Effect of dowel bar position deviation on joint load-transfer ability of cement concrete pavement, Int. J. Pavement Res. Technol. 9 (1) (2016).
[28] M.I. Anastasios, G.T. Korovesis, Analysis and design of doweled slab-on-grade pavement systems, J. Transp. Eng. 118 (6) (1992).
[29] J.R. Roesler, V.G. Cervantes, A.N. Amirkhanian, Accelerated performance testing of concrete pavement with short slabs, Int. J. Pavement Eng. 13 (6) (2012) 494–507, https://doi.org/10.1080/10298436.2011.575134.
[30] S.N. Shoukry, G.W. William, Evaluation of Load Transfer Efficiency Measurement, Mid-Atlantic Universities Transportation Center Final Report, 2005, source at: https://www.researchgate.net/publication/228410739_Evaluation_of_Load_Transfer_Efficiency_Measurement.
[31] M. Coni, S. Portas, R. Isola, J.R.M. Oliveira, FE evaluation of 4-point bending test for fatigue cracking assessment, in: Sixth RILEM International Conference on Cracking in Pavements, Chicago, Illinois, 9–11 June 2008 Chicago, USA.
[32] J.P. Cook, R.M. Lewis, Evaluation of pavement joint and crack sealing materials and practices, NCHRP report n.38, Transp. Res. Board (1967), ISSN: 0077-5614.
[33] A. Kasahara, Estimation of apparent elastic modulus of concrete block layer, in: Proceedings Third Int. Conf. on Concrete Block Paving, Rome (IT), 1988.
[34] Ascher, T. Lerch, M. Oeser, F. Wellner, 3D-FEM simulation of concrete block pavements, in: 8th International Conference on Concrete Block Paving, November 6–8, 2006 San Francisco, California USA D.
[35] I.L. Al-Qadi, S. Portas, M. Coni, S. Lahouar, Runway Pavement Stress and Strain Experimental Measurements, Transportation Research Record, No. 2153, 2010.